Adaptive Motion Planning via Dynamic Constraints Satisfaction

Appendix

Constraint Satisfaction Modeling

We formulate the functions to evaluate the constraint satisfaction in the paper. Here, we classified the relaxable constraints into three categories ($\mathrm{DS}^1(\mathcal{X}_{i,k})$, $\mathrm{DS}^2(\mathcal{X}_{i,k})$, $\mathrm{DS}^3(\mathcal{X}_{i,k})$) based on their relationship with target values, i.e., LESS THAN, MORE THAN and AS CLOSE AS POSSIBLE. $\mathrm{DS}^0(\mathcal{X}_{i,k})$ is to evaluate the satisfaction of unrelaxable constraints. Correspondingly, the functions to evaluate constraint satisfaction are listed as follows:

$$\mathrm{DS}^1(\mathcal{X}_{i,k}) = \begin{cases} 1 & \mathcal{X}_{i,k} \leq g_i \\ \frac{ub_i - \mathcal{X}_{i,k}}{ub_i - g_i} & g_i < \mathcal{X}_{i,k} \leq ub_i \\ 0 & otherwise \end{cases}$$

$$\mathrm{DS}^2(\mathcal{X}_{i,k}) = \begin{cases} \frac{\mathcal{X}_{i,k} - lb_i}{g_i - lb_i} & lb_i \leq \mathcal{X}_{i,k} < g_i \\ 1 & \mathcal{X}_{i,k} \geq g_i \\ 0 & otherwise \end{cases}$$

$$\mathrm{DS}^3(\mathcal{X}_{i,k}) = \begin{cases} \frac{\mathcal{X}_{i,k} - lb_i}{g_i - \sigma_i - lb_i} & lb_i \leq \mathcal{X}_{i,k} < g_i - \sigma_i \\ 1 & g_i - \sigma_i \leq \mathcal{X}_{i,k} \leq g_i + \sigma_i \\ \frac{ub_i - \mathcal{X}_{i,k}}{ub_i - g_i - \sigma_i} & g_i + \sigma_i < \mathcal{X}_{i,k} \leq ub_i \\ 0 & otherwise \end{cases}$$

$$\mathrm{DS}^0(\mathcal{X}_{i,k}) = \begin{cases} 1, & \text{if } \mathcal{X}_{i,k} \text{ satisfies } C_i \in \mathcal{C}_{nr} \\ 0, & \text{otherwise} \end{cases}$$

- Safety: The indicator to evaluate the safety constraint is the collision risk during the mission. Supposing that the obstacles detected by the AMR at time instant k are $\mathcal{O}_k$, while the current state of AMR is s_k. Thus, the QM of safety is $\mathcal{X}_{S_{o,k}} = \frac{\|\boldsymbol{x}_k - \boldsymbol{x}_o\|_2 - r_a - r_o}{D_o}, \forall o \in \mathcal{O}_k$. Such that the average distance between AMR and the center of obstacle reflects the safety risk.

$$\mathrm{DS}^2(\mathcal{X}_{S_{o,k}}) = \begin{cases} 0, & \mathcal{X}_{S_{o,k}} < 0 \\ 1, & \mathcal{X}_{S_{o,k}} \geq 1 \\ \mathcal{X}_{S_{o,k}}, & otherwise \end{cases}$$

- Timelines: The total traveling time from time instant i to j is denoted as $\xi_{ij} = \sum_{k=i}^{j-1} \frac{\|\boldsymbol{x}_{k+1} - \boldsymbol{x}_k\|_2}{\boldsymbol{v}_k}$. The indicator of timeliness is $\mathcal{X}_\xi = \xi_{0T}$, the degree of satisfaction of the timeliness constraint of the whole trajectory $\mathrm{DS}_(\mathcal{X}_\xi)$ is:

$$\mathrm{DS}^1(\mathcal{X}_\xi) = \begin{cases} 1, & \mathcal{X}_\xi \leq \Delta_t \\ \frac{\Delta - \mathcal{X}_\xi}{\Delta - \Delta_t}, & \Delta_t < \mathcal{X}_\xi \leq \Delta \\ 0, & \mathcal{X}_\xi > \Delta \end{cases}$$

- Accuracy: The average quality of the information collected during the mission is denoted as $\mathcal{X}_\varphi = \frac{1}{\xi_{0T}} \sum_{k=0}^{T-1} \|\boldsymbol{w}\| \tau$, the degree of satisfaction is $\mathrm{DS}_(\mathcal{X}_\varphi)$ is:

$$\mathrm{DS}^2(\mathcal{X}_\varphi) = \begin{cases} 0, & \mathcal{X}_\varphi < A \\ \frac{\mathcal{X}_\varphi - A}{A_t - A}, & A \leq \mathcal{X}_\varphi < A_t \\ 1, & \mathcal{X}_\varphi \geq A_t \end{cases}$$

- Energy-saving: The total energy consumption from time instant i to j is denoted as $e_{ij} = \sum_{k=i}^{j-1} \|\boldsymbol{x}_{k+1} - \boldsymbol{x}_k\|_2 + \eta_1 \cdot \|\boldsymbol{v}_{k+1} - \boldsymbol{v}_k\|_2 + \eta_2 \cdot \|\boldsymbol{w}_k\| \tau$. The indicator of energy consumption is $\mathcal{X}_E = e_{0T}$, the degree of satisfaction of energy constraint DS_E is:

$$\mathrm{DS}^1(\mathcal{X}_E) = \begin{cases} 1, & \mathcal{X}_E \leq E_t \\ \frac{E - \mathcal{X}_e}{E - E_t}, & E_t < \mathcal{X}_e \leq E \\ 0, & \mathcal{X}_E > E \end{cases}$$

Experiment Results

We show the details of the experimental results in the quadrotor prototype discussed in the paper.

Scalability To demonstrate the scalability of ACMP for different scales of environments, we further simulate the quadrotor on two selected real urban environments from the open building dataset of Portland in USA (Burian et al. 2002). We used ArcGIS map to set up a 3D model based on the method in (Hidalgo-Panagua et al. 2017). Their original spaces are $500 \times 500 \times 100m^3$ and $10^3 \times 10^3 \times 100\ m^3$, and compressed into $50 \times 50 \times 10\ m^3$ and $100 \times 100 \times 10\ m^3$, respectively. In the dataset, we can also obtain the center of each building's longitude and latitude and its average

Table 1: Adaptive-Constrained Motion Planning Results for Different Scales of Environments

Scale		*Accuracy* [%]	*Traveling Time* [s]	*Energy Consumption* [unit]	*Safety*	*Privacy*	*Real-time Performance*
50	$\mathcal{C}_r$	A_t=90	Δ_t=60	E_t=100	D_o=5m	D_p=10m	Adaptation Rate
	$\mathcal{C}_{nr}$	A=80	Δ=90	E=150	r_o=5m	r_p=5m	6/120
	$\mathcal{X}$	90	60.00	105.57	0	0	Overhead
	$\mathcal{DS}$	100%	100%	88.85%	100%	100%	Avg. 0.066s Std. 0.139s
100	$\mathcal{C}_r$	A_t=90	Δ_t=90	E_t=200	D_o=5m	D_p=10m	Adaptation Rate
	$\mathcal{C}_{nr}$	A=80	Δ=150	E=300	r_o=5m	r_p=5m	3/203
	$\mathcal{X}$	90	101.50	210.94	0	0.1534	Overhead
	$\mathcal{DS}$	100%	80.83%	89.06%	100%	99.98%	Avg. 0.132s Std. 0.180s

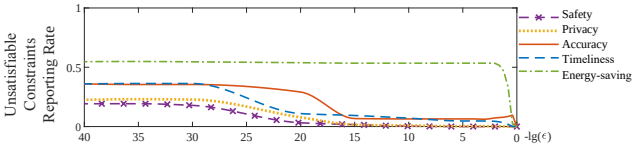

Figure 1: Unsatisfiable constraints reporting rate. (UAV case, $\rho_o = 2\%, \rho_p = 2\%$)

height and building types (i.e., industrial and commercial buildings, houses, and apartments to live in). The buildings for industrial and commercial use are viewed as obstacles, while houses and apartments are viewed as private regions. As shown in Fig. 2, the process of real urban scenario modeling is explained. We set the range of longitude and latitude of working space on the ArcGIS map, and all the buildings are marked as blue (Fig. 2(a)). Then the ArcGIS map is turned into a binary map. Thus a 3D model of the urban scene is set up with the scale of $500m \times 500m \times 100m$ in Fig. 2(c).

In each case, the flight task of the quadrotor is to travel from the position $[0, 0, 0]$ to the destination $[49, 49, 0]$ and $[99, 99, 0]$ respectively. During the flight, the quadrotor is expected to follow constraints of safety, privacy, timeliness, accuracy, and energy-saving. The flight path, velocity, sensor configurations and constraint achievement of the quadrotor at each time instant are shown in Figure 2(d), Figure 2(e) and Figure 2(f). So as to scenario construction for the scale of $1000m \times 1000m \times 100m$ in Figure 3.

Table 1 summarizes the experiment results in these two scales of environment. From our simulation results, in the scale of $50 \times 50 \times 10$, the flight task is completed in 60.07 s, consuming 106.27 units of energy without safety and privacy risk. In the scale of $100 \times 100 \times 10$, the task is finished in 101.5 s, consuming 210.94 units of energy. It does not have safety risk but gets 4 points along the trajectory where relaxable privacy constraint is violated, resulting in an average 99.98% constraints satisfaction along the path. ACMP has high scalability as the two important steps *Constraints Satisfaction Checking* and *Constraints Satisfaction Optimization* are solved by SQP, which can handle large-scale optimization problems. In contrast, SCMP fails to compute a motion plan in real-time when the workspace's size increases.

Choice of violation tolerance Given a set of violation tolerances, the possibilities that relaxable constraints are reported as unsatisfiable are recorded per simulation, as shown in Fig. 1. We choose $\epsilon_{SR,PR,\varphi,\xi,e} = \{10^{-20}, 10^{-20}, 10^{-10}, 10^{-20}, 0.005\}$ in the quadrotor simulation, the possibilities that reporting unsatisfiable relaxable constraints of safety, privacy, timeliness, accuracy, and energy-saving are 16.0%, 14.7%, 29.0%, 25.5%, and 1.1% respectively. These results show that choosing the right violation tolerance parameters can help determine the appropriate set of unsatisfied constraints with a smaller impact on the algorithm's efficiency. In the case that the choice of tolerance parameter may affect the convergence in the *constraints Satisfaction Optimization* step and result in no feasible solutions, ACMP can directly leverage the planning results from the *constraints Satisfaction Checking* step, as illustrated in the Algorithm 1.

UUV Oceanic Surveillance

This example originates from (Shevtsov and Weyns 2016; Shevtsov, Weyns, and Maggio 2019). Rather than considering single-objective optimization for the UUV scenario in (Shevtsov and Weyns 2016; Shevtsov, Weyns, and Maggio 2019), we extended it to achieve multiple constraints under uncertainties and disturbances, while other parameters like sensor configurations are kept the same as (Shevtsov and Weyns 2016), as shown in Table 2. The constraints to achieve in this scenario are listed as follows:

- Scanning Distance (C_l): A segment of the surface over a distance of $L_t = 100$ km is expected to be examined by the UUV within $\Delta = 10$ hours, while the unrelaxable constraint of surveillance distance is $L = 90$ km.
- Energy Consumption (C_E): A total amount of energy $E_t = 5.4$ MJ is expected to be consumed, while the maximum amount of energy is $E = 6$ MJ.
- Accuracy (C_φ): The accuracy of sensor measurements is targeted at $A_t = 90\%$, while the unrelaxable accuracy constraint is set as $A = 80\%$.

Constraints Satisfaction Modeling

The UUV is equipped with 5 sensors for ocean surveillance. The scanning time 10 hours is 360 time instance,

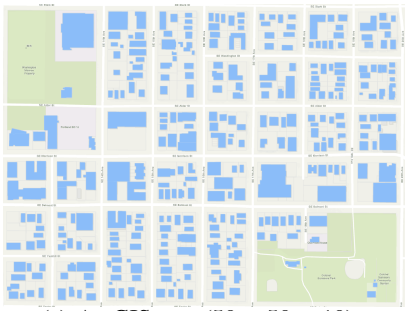

(a) ArcGIS map ($50 \times 50 \times 10$).

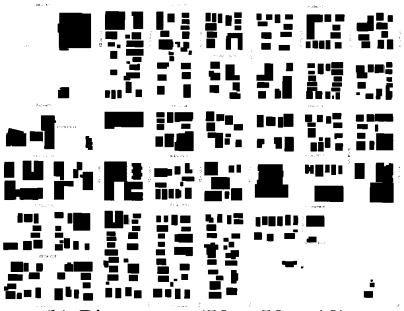

(b) Binary map ($50 \times 50 \times 10$).

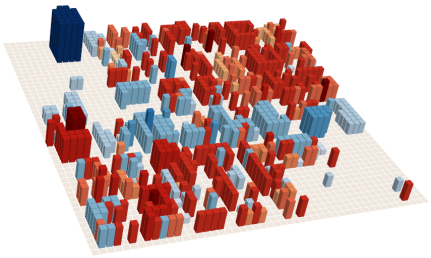

(c) Grid map ($50 \times 50 \times 10$).

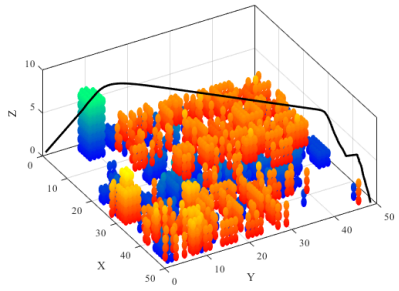

(d) Flight path of the quadrotor.

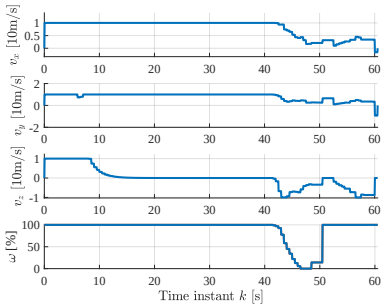

(e) Velocity and sensor configurations.

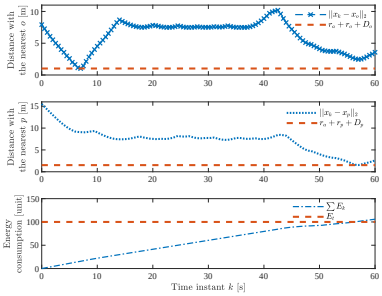

(f) Constraint satisfaction during the flight.

Figure 2: Environment modeling with the scale of $500m \times 500m \times 100m$.

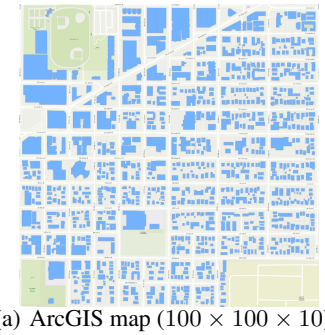

(a) ArcGIS map ($100 \times 100 \times 10$).

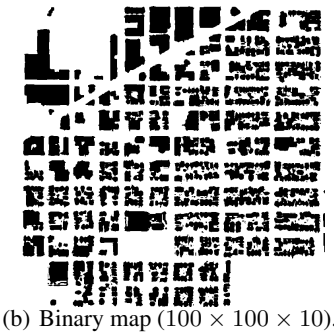

(b) Binary map ($100 \times 100 \times 10$).

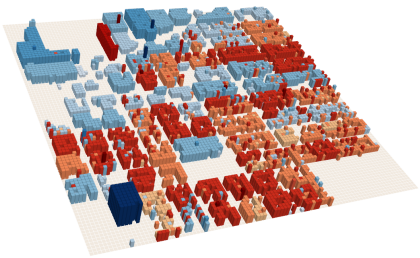

(c) Grid map ($100 \times 100 \times 10$).

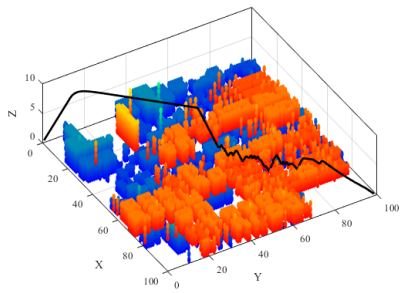

(d) Flight path of the quadrotor.

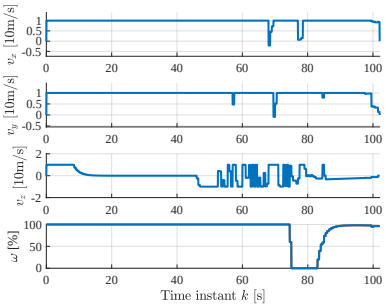

(e) Velocity and sensor configurations.

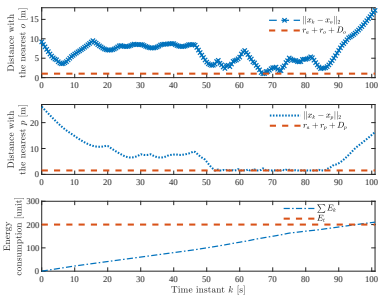

(f) Constraint satisfaction during the flight.

Figure 3: Environment modeling with the scale of $1000m \times 1000m \times 100m$.

Table 2: Parameters of sensors of the UUV.

UUV onboard sensor	Energy cons. J/s	Scan Speed m/s	Accuracy %
1	170	2.6	97
2	135	3.6	89
3	118	2.6	83
4	100	3.0	74
5	78	3.6	49

$x_i, i \in [1, 5]$ is the portion of time the sensor i should be used during system operation in each instance. Acc_i is the accuracy of sensor i; E_i is the energy consumed by sensor; V_i is the scanning speed of sensor. q_i is portion of accuracy of sensor and p_i is for scanning speed respectively in decimals. The energy consumed is related with working accuracy and speed of sensor. The corresponding quantification measures are computed as: $\mathcal{X}_l = \sum_{k=0}^{T}\sum_{i=0}^{N} x_i q_i V_i \tau$, $\mathcal{X}_E = \sum_{k=0}^{T}\sum_{i=0}^{N} x_i E_i \cdot \frac{e^{p_i+q_i}-1}{e^2-1}\tau$, and $\mathcal{X}_\varphi = \sum_{k=0}^{T}\sum_{i=0}^{N} x_i p_i Acc_i$, where $T = 360$, i.e., the time interval is 100s and the time instance k incremented by $1 \sim 100$. The constraint satisfaction functions are shown as follows:

- Scanning distance (C_l):

$$\mathrm{DS}^2(\mathcal{X}_l) = \begin{cases} 0, & \mathcal{X}_l < L \\ \dfrac{\mathcal{X}_l - L}{L_t - L}, & L \le \mathcal{X}_l < L_t \\ 1, & \mathcal{X}_l \ge L_t \end{cases}$$

- Energy consumption (C_E):

$$\mathrm{DS}^1(\mathcal{X}_E) = \begin{cases} 1, & \mathcal{X}_E \le E_t \\ \dfrac{E - \mathcal{X}_E}{E - E_t}, & E_t < \mathcal{X}_E \le E \\ 0, & \mathcal{X}_E > E \end{cases}$$

- Accuracy (C_φ):

$$\mathrm{DS}^2(\mathcal{X}_\varphi) = \begin{cases} 0, & \mathcal{X}_\varphi < A \\ \dfrac{\mathcal{X}_\varphi - A}{A_t - A}, & A \le \mathcal{X}_{\varphi_k} < A_t \\ 1, & \mathcal{X}_\varphi \ge A_t \end{cases}$$

Experiment Results

To demonstrate the generality of ACMP, we applied it to a UUV case described in (Shevtsov and Weyns 2016). The constraint satisfaction functions in this scenario are $\mathrm{DS}^1(\mathcal{X}_l)$ (scanning distance), $\mathrm{DS}^2(\mathcal{X}_E)$ (energy consumption) and $\mathrm{DS}^2(\mathcal{X}_\varphi)$ (accuracy). There are trade-offs between the satisfaction of these constraints, e.g., when sensors (e.g., sensor 1) with a higher quality of surveillance is chosen, more energy is consumed, resulting in less distance scanned.

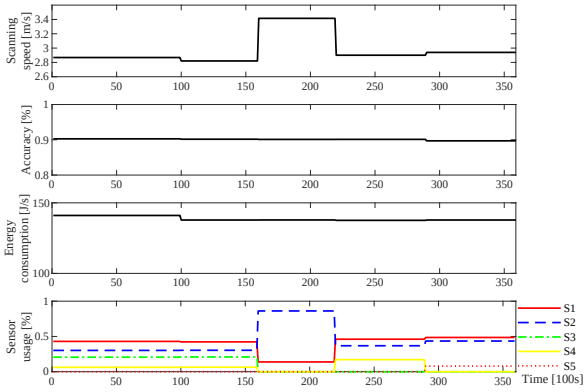

Figure 4: Adaptive-Constrained Motion Planning Results in the UUV Case.

Table 3: Constraints Satisfaction Results in the UUV Case.

QMs.	*Approaches*	# of disturbances				
		3	6	9	12	15
$\mathcal{X}_\varphi$ [%]	SCMP	88.9	87.5	85.8	84.4	82.4
	ACMP	***89.6***	***88.4***	***87.0***	***85.4***	***83.2***
$\mathcal{X}_l$ [km]	SCMP	99.9	99.2	98.0	96.6	94.5
	ACMP	***104.2***	***104.0***	***103.5***	***101.0***	***98.9***
$\mathcal{X}_E$ [MJ]	SCMP	5.34	5.33	5.31	5.34	5.34
	ACMP	***5.24***	***5.18***	***5.14***	***5.16***	***5.16***

[a] The violation tolerance are $\epsilon_\varphi = 10^{-3}$, $\epsilon_l = 0$, and $\epsilon_e = 0$.

Effectiveness The Fig. 4 shows the adaptive constrained motion planning results of the UUV during operation with the case in (Shevtsov and Weyns 2016). At $k = 100$, we change the target energy consumption (E_t) from 5.4 to 5.0 MJ; at $k = 160$, we change the distance expected to be scanned (L_t) from 100 to 105 km. The plots show that these changes in constraints lead to corresponding changes in the sensor usage arrangement, as the time portion for $S2$ increases. Figure 4 also shows how ACMP reacts to changes in sensor parameters and sensor failures. At $k = 220$, the measurement accuracy of sensor $S3$ drastically decreases from 83% to 43%, at $k = 290$, $S4$ stops working, and leads to an optimal solution that $S1$ is more exploited. Finally, the mission end with average measurement accuracy at 90.1%, scanning distance at 106.7 km, and energy consumption at 4.98 MJ.

Robustness In this scenario, the performance of ACMP and SCMP is compared while adding disturbances to sensors' parameters at random time instants, i.e., sensor accuracy, scanning speed, and energy consumption. For each frequency of disturbances, we simulated 500 rounds and computed the average accuracy, scanning distance, and energy consumption. The results are shown in Table 3. We can see that under ACMP, the UUV can scan a longer distance with higher accuracy and less energy consumption than SCMP. Moreover, the motion generated by SCMP can hardly sat-

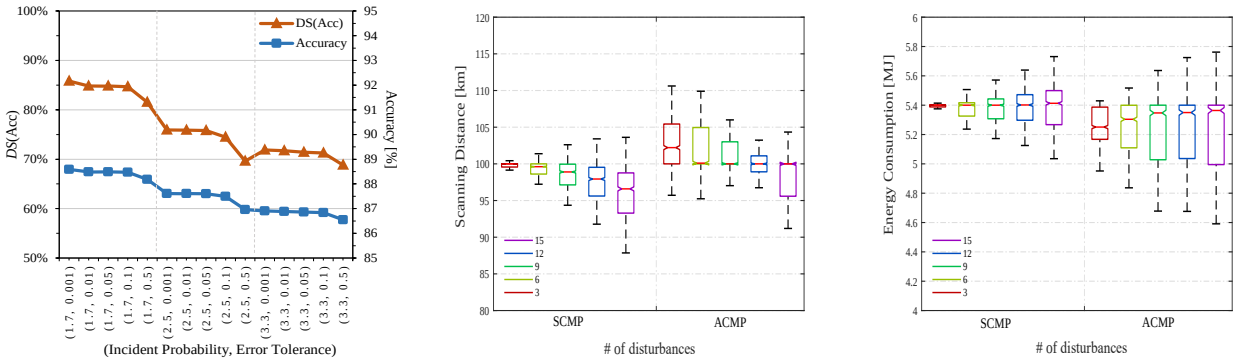

(a) Scanning accuracy with various disturbances and ϵ. (ACMP)

(b) Variance of scanning distance.

(c) Variance of energy consumption.

Figure 5: Scanning accuracy, distance and energy consumption with various probability of disturbances and violation tolerance.

isfy all the three constraints, while the motion generated by ACMP can satisfy the timeliness and energy constraints, only slightly violating the accuracy constraint. The reason behind this is that at the *Constraints Satisfaction Analysis* stage, the accuracy is selected as the objective function to optimize while the other two remain as their original formula as constraints. The variance of scanning distance and energy consumption of two strategies are compared in Figure 5(b) and Figure 5(c).

Table 4: Statistics on Overhead Data.

Cases	***Approaches***	***Average*** [s]	***Standard Deviation*** [s]
Quadrotor	SCMP	0.2115	0.0879
	ACMP	***0.0811***	***0.0821***
UUV	SCMP	0.0423	0.0092
	ACMP	***0.0344***	***0.0217***

Real-time Performance Finally, we analyze the computation overhead of ACMP in generating an optimal self-adaptive plan. Table 4 shows the empirical distribution of the computation time for 10000 executions of each method in either simulation. From Table 4, the difference in average computation time between SCMP and ACMP is about 7 ms (0.0423 s versus 0.0344 s) in the UUV case and 130 ms (0.2115 s versus 0.0811 s) in the UAV case.

This result is because SCMP considers the optimization of all relaxable constraints while ACMP only considers the optimization of relaxable constraints that are predicted cannot be satisfied. So SCMP requires more computation, especially when there are more relaxable constraints to be considered. ACMP has a larger variance since the number of objective functions to be optimized may vary at runtime. In the worst case, when all the relaxable constraints need to be adjusted, the computation time of ACMP will be larger than SCMP. This case is very rare from our experiment results. Hence, ACMP is flexible and capable of accommodating multiple constraints at runtime.

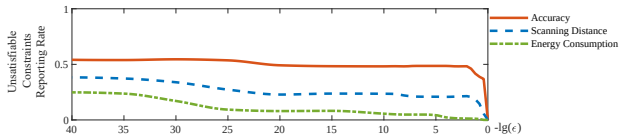

Figure 6: Unsatisfiable constraints reporting rate. (UUV case, # of disturbances = 9)

Choice of violation tolerance As discussed in the paper, the choice of violation tolerances $\boldsymbol{\epsilon}$ determines which constraint needs relaxation, while the larger the value is, the less number of constraints in the ε-unsatisfiable constraints set, along with the underlying higher risk of no feasible solution in the step of *Constraints Satisfaction Optimization*. Thus the value of $\boldsymbol{\epsilon}$ should be delicately determined based on experimental data. The relationship between different violation tolerance and accuracy constraint satisfaction is illustrated in Figure 5(a). As the number of disturbances increases, the impact of ϵ on constraint satisfaction is more obvious. Figure 6 illustrates the possibilities that relaxable constraints are reported as unsatisfiable in the UUV case, as the increase of violation tolerance increases. In the UUV case, we choose $\epsilon_{l,E,\varphi} = \{0, 0, 10^{-3}\}$, when the possibility of reporting unsatisfiable constraints tends to be gentle.

References

Burian, S. J.; Velugubantla, S. P.; Chittineni, K.; Maddula, S. R. K.; and Brown, M. J. 2002. Morphological analyses using 3D building databases: Portland, Oregon. Technical report, Utah. LA-UR, Los Alamos National Laboratory, Los Alamos, NM.

Hidalgo-Panagua, A.; Vega-Rodríguez, M. A.; Ferruz, J.; and Pavón, N. 2017. Solving the multi-objective path planning problem in mobile robotics with a firefly-based approach. *Soft Computing* 21(4): 949–964.

Shevtsov, S.; and Weyns, D. 2016. Keep it simplex: Satisfying multiple goals with guarantees in control-based self-

adaptive systems. In *Proceedings of the 2016 24th ACM SIGSOFT International Symposium on Foundations of Software Engineering*, 229–241. ACM.

Shevtsov, S.; Weyns, D.; and Maggio, M. 2019. SimCA*: A control-theoretic approach to handle uncertainty in self-adaptive systems with guarantees. *ACM Transactions on Autonomous and Adaptive Systems (TAAS)* 13(4): 17.